Supporting Information

Copper substituted $NiTiO_3$ Ilmenite type Materials for Oxygen Evolution Reaction

*Amandine Guiet, ‡[1] Tran Ngoc Huan, ‡[2] Christophe Payen,[3] Florence Porcher,[4] Victor Mougel,[2,5] Marc Fontecave, *[2] Gwenaël Corbel *[1]*

[1] Institut des Molécules et Matériaux du Mans, UMR 6283 CNRS, Le Mans Université, Avenue Olivier Messiaen, 72085 Le Mans Cedex 9, France

[2] Laboratoire de Chimie des Processus Biologiques, Collège de France, UMR CNRS 8229, Sorbonne Université, PSL Research University, 11 place Marcelin Berthelot, 75005 Paris, France

[3] Institut des Matériaux Jean Rouxel (IMN), Université de Nantes, CNRS, 2 rue de la Houssinière, BP 32229, 44322 Nantes cedex 3, France

[4] Laboratoire Léon Brillouin, CEA-CNRS, 91191 Gif-sur-Yvette Cedex, France

[5] Present address: Department of Chemistry and Applied Biosciences, Eidgenössische Technische Hochschule Zürich, 8093 Zurich, Switzerland.

‡ both authors contributed equally to this study

* corresponding authors

*E-mail:marc.fontecave@college-de-france.fr

*E-mail:gwenael.corbel@univ-lemans.fr

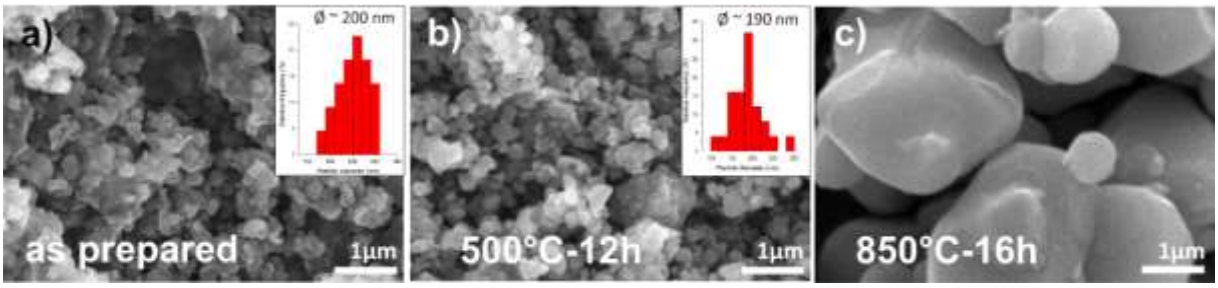

Figure S1: Synthesis of $Ni_{0.8}Cu_{0.2}TiO_3$ powder from a mixture of copper and nickel nitrates: SEM pictures of the as-prepared nitrate mixture (a) and after its calcination in air at 500°C for 12h (b). (c) SEM picture of $Ni_{0.8}Cu_{0.2}TiO_3$ powder after subsequent calcination in air at 850°C for 16h.

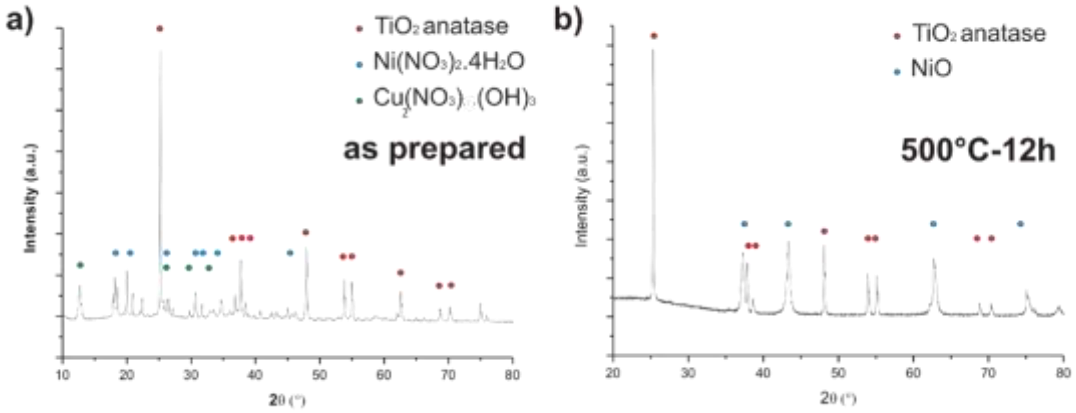

Figure S2: Synthesis of $Ni_{0.8}Cu_{0.2}TiO_3$ powder from a mixture of copper and nickel nitrates: XRPD pattern of the as-prepared mixture (a) and (b) after its calcination in air at 500°C for 12h (b).

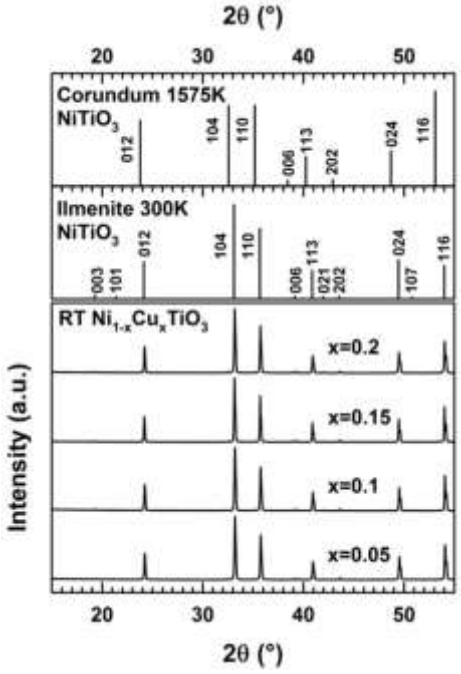

Figure S3: XRPD patterns of $Ni_{1-x}Cu_xTiO_3$ raw powders collected at room temperature ($CuK\alpha_{1+2}$ radiations). Comparison of the XRPD patterns of the Ilmenite form of $NiTiO_3$at 300K with that of the its Corundum form at 1575K, both calculated from crystallographic data published in reference[1]with the $CuK\alpha_1$ radiation wavelength.

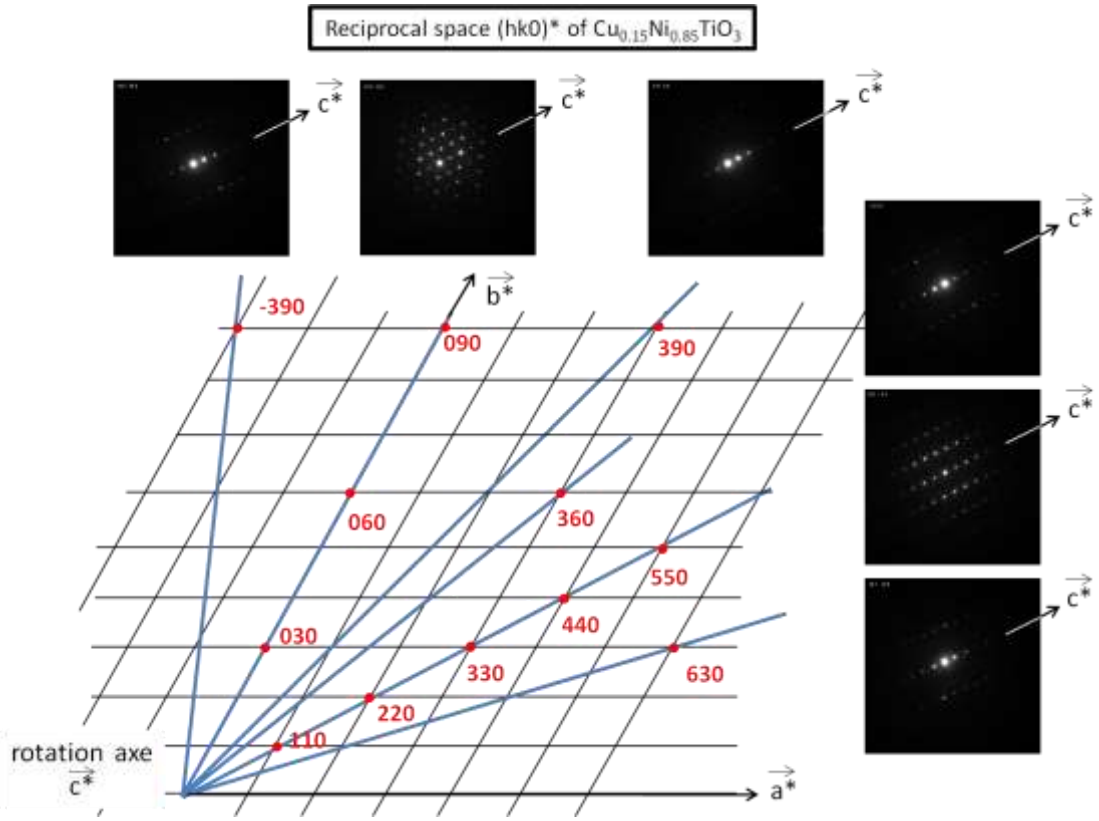

Figure S4: Reconstitution of the reciprocal space of $Ni_{0.85}Cu_{0.15}TiO_3$

Table S1: Results of Rietveld refinement for $Ni_{1-x}Cu_xTiO_3$ (Space group *R-3* (n°148)) carried out with the structural model 1 from Neutron Powder Diffraction data collected at room temperature. For each composition, lattice parameters, positions coordinates, equivalent isotropic temperature factors and site occupancy factors are listed as well as R-factors for the fit.

		x	**0.05**	**0.10**	**0.15**	**0.20**
		a (Å)	5.03295(3)	5.03371(3)	5.03469(3)	5.03599(3)
		c (Å)	13.7963(2)	13.7975(2)	13.7997(2)	13.8017(2)
Atom	**Multiplicity and Wyckoff letter**	**Positions Coordinates**	**0.05**	**0.10**	**0.15**	**0.20**
Cu	6c	z	0.3507(2)	0.3509(2)	0.3510(1)	0.3512(2)
		$B_{eq.}$ (Å^2)	0.3163	0.1211	0.0681	0.3778
		Occupancy	0.05	0.1	0.15	0.2
Ni	6c	z	0.3507(2)	0.3509(2)	0.3510(1)	0.3512(2)
		$B_{eq.}$ (Å^2)	0.3163	0.1211	0.0681	0.3778
		Occupancy	0.95	0.9	0.85	0.8
Ti	6c	z	0.1445(5)	0.1443(3)	0.1445(4)	0.1447(5)
		$B_{eq.}$ (Å^2)	0.3163	0.1211	0.0681	0.3778
		Occupancy	1	1	1	1
O	18f	x	0.3155(6)	0.3151(5)	0.3155(5)	0.3155(6)
		y	0.0169(5)	0.0165(4)	0.0169(4)	0.0173(5)
		z	0.2465(2)	0.2466(1)	0.2465(1)	0.2464(2)
		$B_{eq.}$ (Å^2)	0.3683	0.2042	0.1566	0.4848
		Occupancy	1	1	1	1
		Number of reflections	192	192	192	192
		Rwp (%)	7.08	5.71	5.80	6.88
		Rexp (%)	1.74	1.91	1.72	1.84
		RBragg (%)	2.62	1.59	1.80	2.53
		Rf (%)	1.30	0.894	0.898	1.29

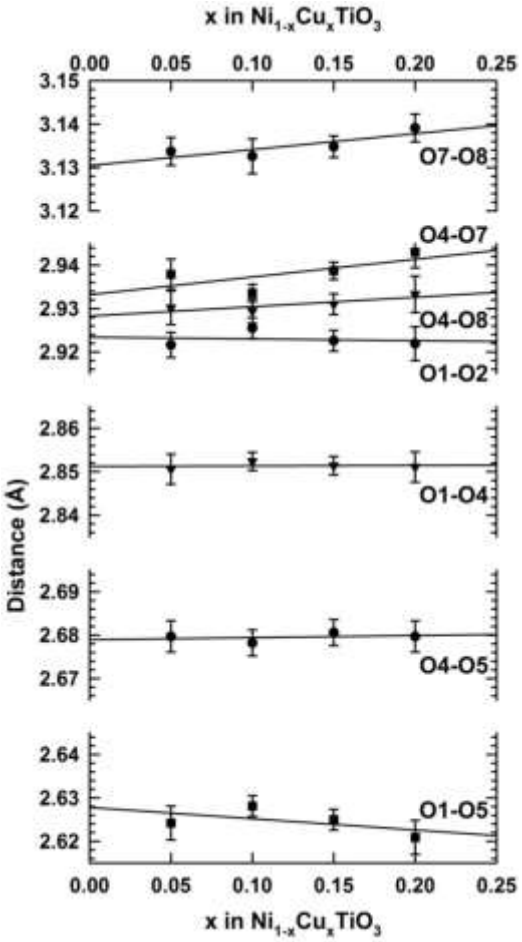

Figure S5: Evolution with the copper content x of the oxygen-oxygen distances in $Ni_{1-x}Cu_xTiO_3$ samples. All these values have been calculated from the crystallographic data reported in ESI Table 1. The values calculated from the crystallographic data of $NiTiO_3$ (x=0)[1] are added for reference (open symbols).

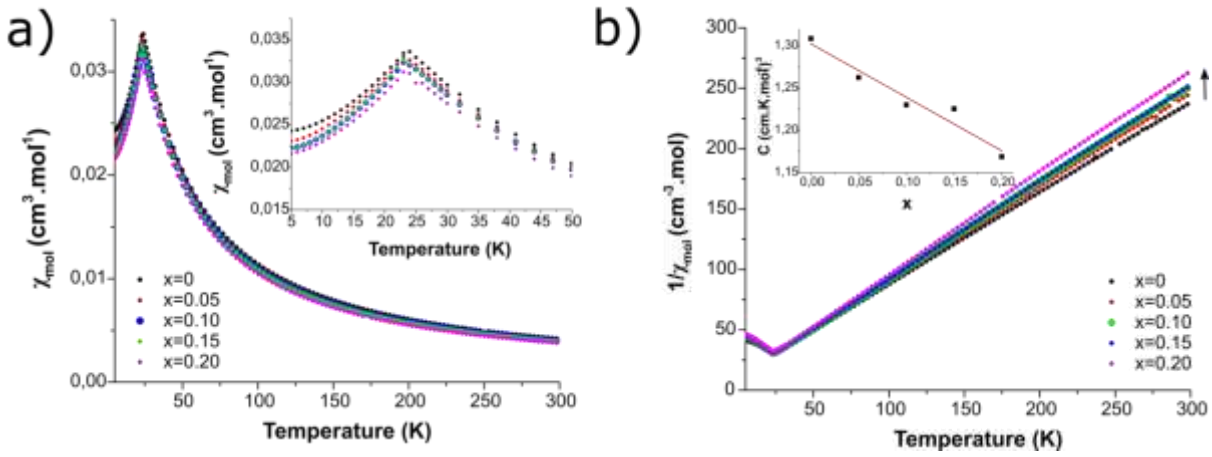

Figure S6: Magnetic properties of micrometric powder samples of $Ni_{1-x}Cu_xTiO_3$ ($0 \leq x \leq 0.2$).a) Temperature dependence of the zero-field cooled magnetic susceptibility χb) Inverse magnetic susceptibly $1/\chi$ versus temperature. The inset shows the variation of the molar Curie constant *C* as a function of x.

Table S2: Neel temperatures, T_N, molar Curie constants, C, and Weiss temperatures θ of micrometric powder samples of $Ni_{1-x}Cu_xTiO_3$ ($0 \leq x \leq 0.2$).

x	T_N (K)	C($cm^3.K.mol^{-1}$)	θ (K)
0	24.0(5)	1.31(1)	-14.7(1)
0.05	23.0(5)	1.26(1)	-13.2(1)
0.10	23.0(5)	1.23(1)	-12.7(1)
0.15	23.0(5)	1.22(1)	-12.5(1)
0.20	23.0(5)	1.17(1)	-11.6(1)

In pure $NiTiO_3$, Ni^{2+} (S=1) magnetic moments order in a layered antiferromagnetic structure below the Néel temperature $T_N \approx 23K$ (Ti^{4+} ions are diamagnetic ions).[2,3] As observed in $Co_xNi_{1-x}TiO_3$,[4] Cu/Ni substitution has no effect on the Néel temperature T_N for low substitution rates $x \leq 0.2$. In the 30 − 300 K temperature range, however, paramagnetic susceptibilities of $Ni_{1-x}Cu_xTiO_3$ obey a Curie−Weiss law, $\chi(x,T) = C(x)/[T - \theta(x)]$ with monotonous dependencies of the molar Curie Constant C and of the Weiss temperature θ with respect to the substitution rate x. The observed linear decrease of the molar Curie constant with increasing Cu content is fully consistent with chemical substitution of S=1/2 Cu^{2+} magnetic moments for S=1 Ni^{2+} ions.

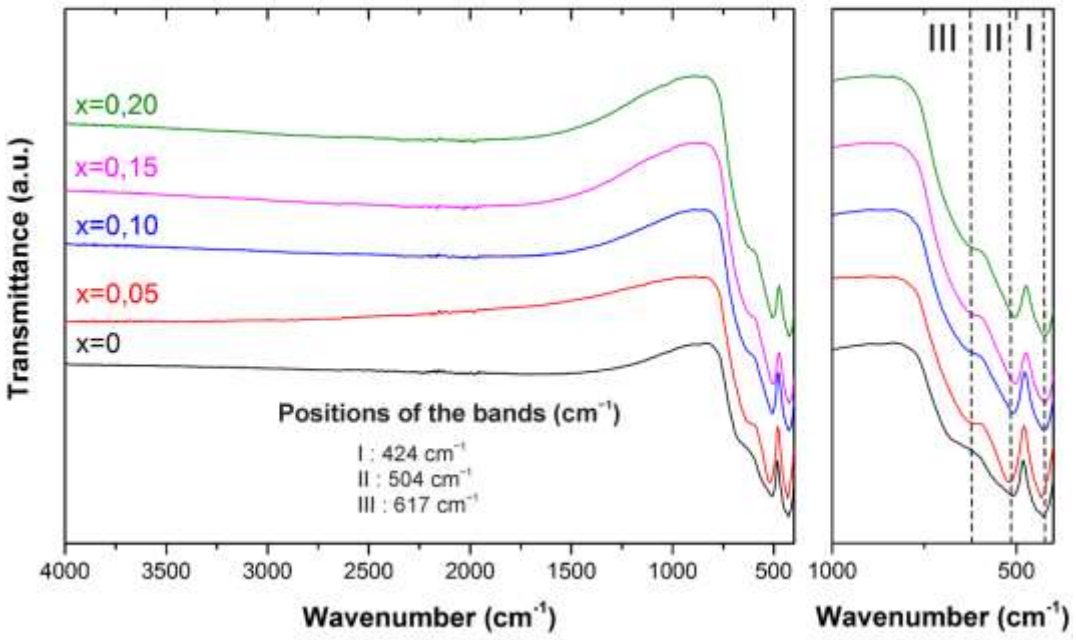

Figure S7: FT-IR spectra of different $Ni_{1-x}Cu_xTiO_3$ sample powders.

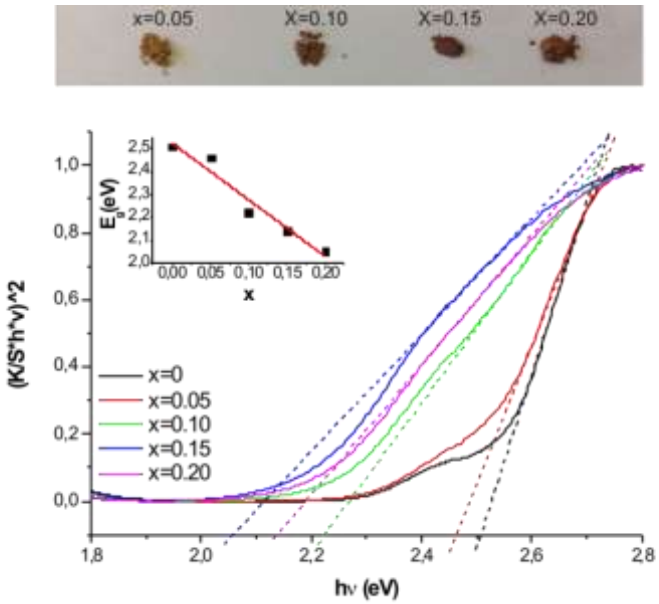

Figure S8: *On the top*: Pictures of the $Ni_{1-x}Cu_xTiO_3$ powders. *Graph:* Tauc plots (calculated as indirect band gap) obtained for the different $Ni_{1-x}Cu_xTiO_3$ materials. Inset: linear decrease of the band gap with the value of x.

The Kubelka–Munk function $F(R_{inf})$ is introduced and depends on the K–M effective absorption coefficient (K) and the K– M effective scattering coefficient (S) (equation (1)):

$$F(R_{inf}) = \frac{(1-R_{inf})^2}{2R_{inf}} = \frac{K}{S} \quad (1)$$

The K–M effective absorption coefficient (K) is proportional to the usual absorption coefficient (α) according to K= εα and the K–M effective scattering coefficient (S) is related to the usual scattering coefficient (s) by S=2(1-ς)s. When the material scatters in a perfectly diffuse manner, the K–M effective absorption coefficient (K) becomes K=2α and the K–M effective scattering coefficient (S) is exactly the same as the usual scattering coefficient (s), S=s. Under this condition, the followed expression can be used (equation (2)):

$$[F(R)h\nu]^2 = C_1(h\nu - E_g) \quad (2)$$

Table S3: Results of Le Bail refinement for $Ni_{0.8}Cu_{0.2}TiO_3$-nano (Space group *R-3* (n°148)) carried out with the unit cell parameters and space group of an Ilmenite type structure from X-ray Powder Diffraction data collected at room temperature.

	a	**c**	**Rp**	**Rwp**	**χ^2**	**integral-breadth apparent size ε_β (nm)**	**volume-weighted mean diameter $<D_v>$ (nm)**
$Ni_{0.8}Cu_{0.2}TiO_3$ nano	5.0321(5)	13.806(1)	15.2	10.4	1.64	11.5	15

Table S4: BET surface area (SA_{BET}) of the $Ni_{1-x}Cu_xTiO_3$ nanomaterials

	x=0	x=0.05	x=0.10	x=0.15	x=0.20
SA_{BET} ($m^2.g^{-1}$)	21	29	29	34	32

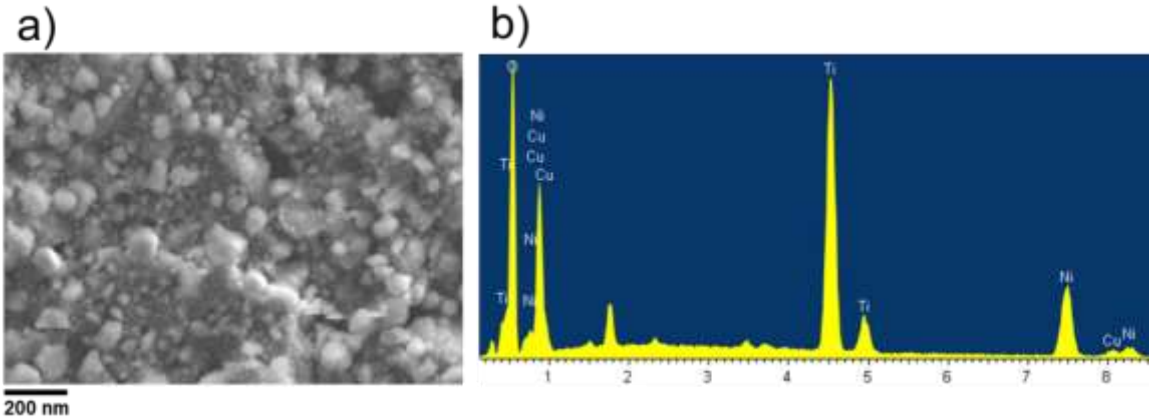

Figure S9: SEM image (a) and corresponding EDX spectrum (b) with elemental mapping of $Ni_{0.8}Cu_{0.2}TiO_3$-nanodeposited on an electrode surface.

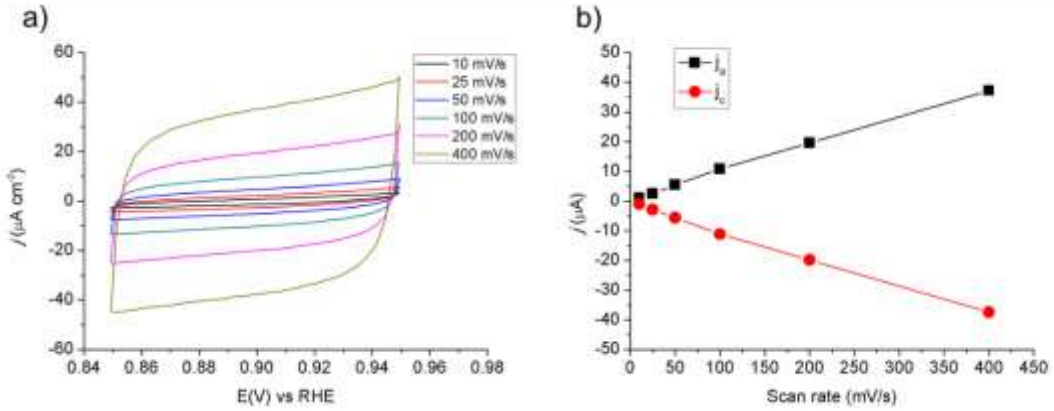

Figure S10: CV of $Ni_{0.8}Cu_{0.2}TiO_3$-nano in KOH 0.1 M at different scan rates (a) and the corresponding capacitance currents (anodic-cathodic) as a function of scan rates.

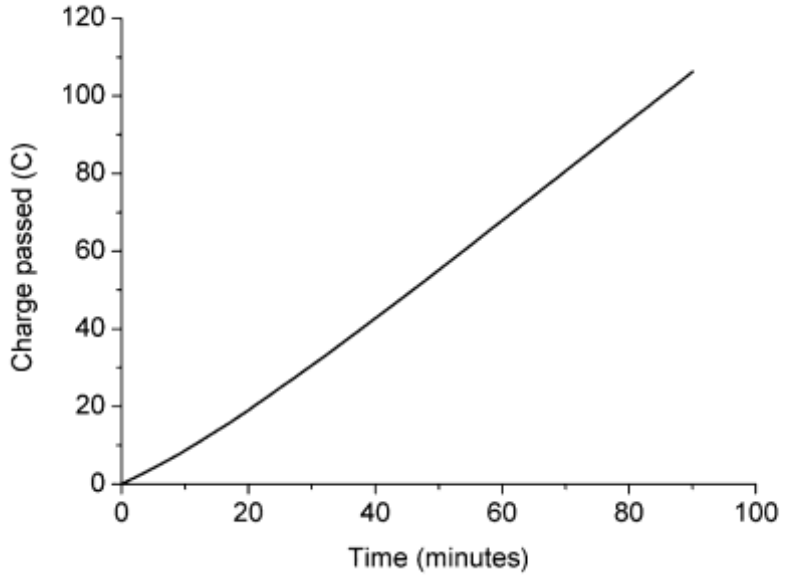

Figure S11: Charge passed during a 90 minutes electrolysis at an applied potential of 1.78 V vs RHE in 0.1 M NaOH solution.

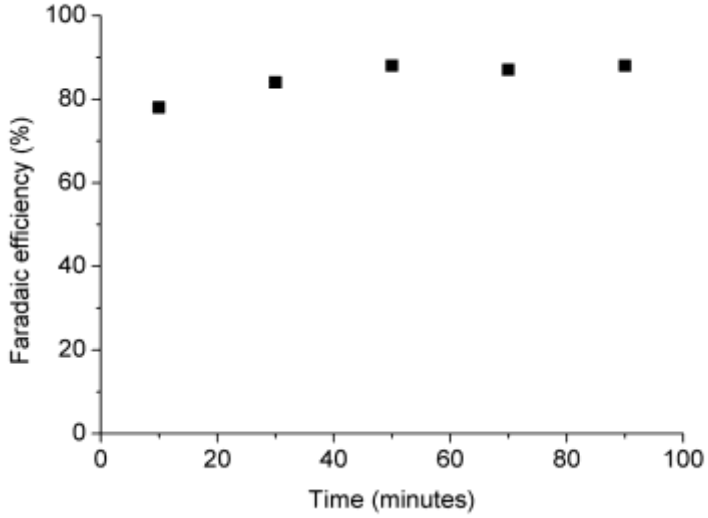

Figure S12: Faradaic efficiency for OER during a 90 minutes electrolysis at 1.78 V vs RHE in 0.1 M NaOH solution.

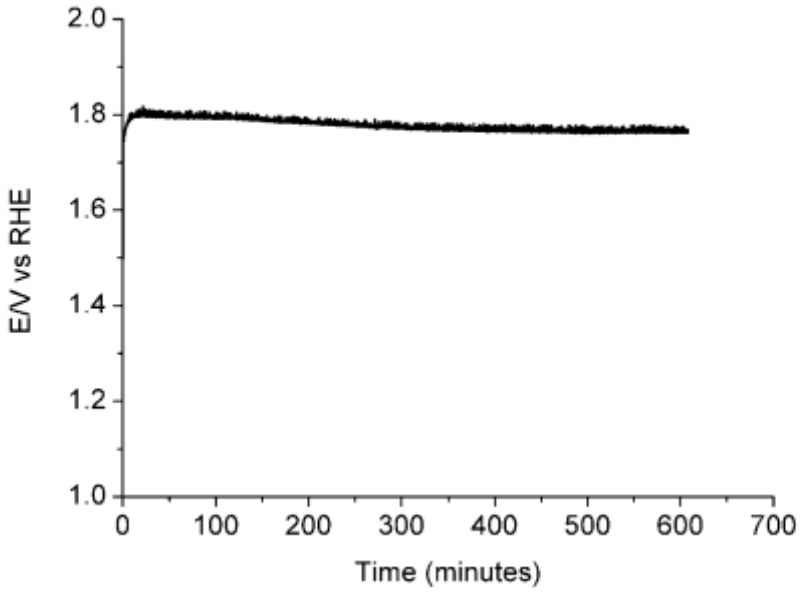

Figure S13: Long term electrolysis at 10.0 mA for O_2 evolution of $Ni_{0.8}Cu_{0.2}TiO_3$-nano/Cu plate in 0.1 M NaOH solution.

Table S5: Comparison the activity of water oxidation of different electrocatalysts that contains Ti in the composition.

Catalysts	**Electrolytes**	**η(mV) at 10mA**	**Reference**
$CoO_x/Co/TiO_2$	1.0 KOH	352	*ACS Catal.*, **2018**, *8* (5), pp 4278–4287
$Co_{0.2}Ni_{0.8}TiO_3$	0.1M NaOH	670	*ACS Appl. Mater. Interfaces***2017**, 9, 40290-40297
$NiO\text{-}TiO_2$	1.0 KOH	330	*J. Am. Chem. Soc.*, **2016**, *138* (20), pp 6517–6524
$NiTe_2$/Ti mesh	1.0 M KOH	315	*ChemElectroChem***2018**, 5(8), 1153–1158
$SrCo_{0.9}Ti_{0.1}O_{3-\delta}$	0.1 M KOH	490	*ACS Appl. Mater. Interfaces*, **2015**, *7* (32), pp 17663–17670
$Cu_2Se\text{-}Cu_2O/Ti$	0.2 M Na2CO3	485	*Chem. Commun.*, **2018**,54, 4979-4982
$TiFeS_x$	1.0 KOH	350	*J. Mater. Chem. A,* **2018**,6, 21891-21895
$Ni_{0.8}Cu_{0.2}TiO_3$-nano	1.0 M NaOH	345	This report
$Ni_{0.8}Cu_{0.2}TiO_3$-nano	0.1 M NaOH	470	This report

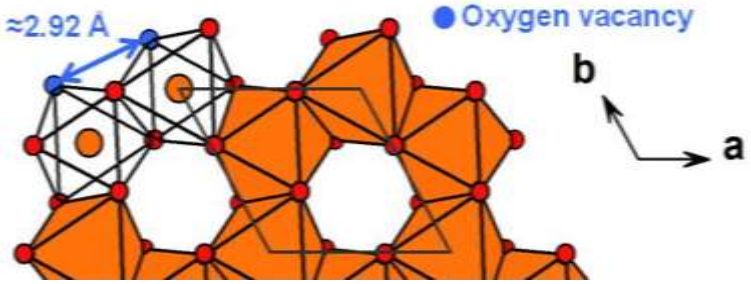

Figure S14: Possible neighboring vacant oxygen positions at terminated honeycomb C1-type layer suitable for adsorption of two OH^- groups in Langmuir-Hinshelwood (LH) mechanism-type OER (shortest O-O distance).

REFERENCES

(1) Boysen, H.; Frey, F.; Lerch, M.; Vogt, T. A Neutron Powder Investigation of High Temperature Phase Transition $NiTiO_3$. *Zeitschrift für Krist.***1995**, *210*, 328–337.

(2) Shirane, G.; J. Pickart, S.; Ishikawa, Y. Neutron Diffraction Study of Antiferromagnetic MnTiO3 and $NiTiO_3$. *J. Phys. Soc. Japan***1959**, *14* (10), 1352–1360. https://doi.org/10.1143/JPSJ.14.1352.

(3) Heller, G. S.; Stickler, J. J.; Kern, S.; Wold, A. Antiferromagnetism in $NiTiO_3$. *J. Appl. Phys.***1963**, *34* (4), 1033–1034. https://doi.org/10.1063/1.1729357.

(4) Watanabe, H.; Yamauchi, H.; Takei, H. Magnetic Anisotropies in $MTiO_3$ (M=Co,Ni). *J. Magn. Mater.***1980**, *3* (15–18), 549–550.